Appl. Phys. A (2016) 122:458
DOI 10.1007/s00339-016-9983-0

Applied Physics A
Materials Science & Processing

Room-temperature rf-magnetron sputter-deposited W-doped indium oxide: decoupling the influence of W dopant and O vacancies on the film properties

Ivan G. Samatov[1] · Bjarke R. Jeppesen[1,2] · Arne Nylandsted Larsen[1,2] · Sanjay K. Ram[1,2]

Received: 10 November 2015 / Accepted: 9 March 2016 / Published online: 29 March 2016

Abstract Tungsten-doped indium oxide (IWO) thin films were deposited at room temperature using rf-magnetron sputtering. The optical, electrical, and structural properties of the IWO films were studied as functions of the O_2-dilution fraction in the Ar sputtering gas. The W-doping level, and contributions of intrinsic oxygen vacancies and W dopant to the free carrier concentration were studied. Windows of optimum deposition conditions are demonstrated where amorphous and smooth-surfaced IWO films are obtained with low resistivity of 3.5×10^{-4} Ω cm, high mobility of 45 $cm^2\ v^{-1}\ s^{-1}$, and high optical transparency (visible and NIR transparencies of 83 and 80 %, respectively). The observed optoelectronic properties are discussed in light of the underlying electron transport mechanisms.

1 Introduction

Applications like flexible electronics and thin-film solar cells have created a need for room-temperature fabrication of transparent electrodes [1, 2]. Tin-doped In_2O_3 (ITO), doped SnO_2, doped ZnO, and more recently transition metal-doped In_2O_3-based materials have shown useful optoelectronic properties for various transparent conducting oxide (TCO) applications [1, 3–6]. In_2O_3-based materials doped with transition metals, such as W, Mo, and Ti, in particular have demonstrated the potential for low resistivity and a high near-infrared (NIR) transmittance due to suitable valence electron configurations, and resultant high mobility even at low doping levels [5, 7, 8], making them attractive for multi-junction solar cells [9], and solar cell light management strategies based on up-conversion of infrared light into visible light [10]. However, these materials are deposited at high temperatures, and obtaining equally good properties in In_2O_3-based materials at room temperatures is a challenge [2, 3]. Further, for room-temperature-deposited W-doped In_2O_3 material (In_2O_3:W, referred to as IWO henceforth), activation of the dopant at low temperatures is difficult [11–13]. This not only affects the electrical properties, but also hinders our understanding of the properties because oxygen vacancies are a significant source of free electrons in this material [2, 13, 14], and it is difficult to determine the exact contribution of the dopants to the observed electrical properties.

For a better understanding of the contribution of the dopant to the microstructural and optoelectronic properties of the IWO system, the effects of the dopant need to be distinguished from those arising from oxygen vacancies, but studies of room-temperature-deposited IWO films showing the effect of variable oxygen concentration for different dopant levels are sparse [15, 16]. In the present study, we have deposited In_2O_3 and IWO thin films using a radio frequency magnetron sputtering (rf-MS) system at room temperature with different W dopant concentrations and different oxygen dilutions for each doping level. We have studied the interplay between the W concentration and the oxygen dilution fraction on the properties of In_2O_3 and IWO films, and in particular sought to isolate out the concentrations of free carriers generated from the ionized dopant atoms and the oxygen vacancies.

✉ Ivan G. Samatov
samatov@inano.au.dk

[1] Interdisciplinary Nanoscience Center, Aarhus University, The iNANO House, Gustav Wieds Vej 14, Building 1590, Office 151, 8000 Aarhus C, Denmark

[2] Department of Physics and Astronomy, Aarhus University, Ny Munkegade 120, 8000 Aarhus C, Denmark

2 Experimental detail

Tungsten-doped and undoped In_2O_3 thin films were deposited on <100> oriented crystalline silicon and borosilicate glass substrates using 13.6 MHz radio frequency magnetron sputtering (AJA ATC ORION system) at room temperature with argon as sputtering gas. The sputtering was performed in confocal geometry with the target-substrate distance fixed at 10 cm and the tilt angle of the magnetron at 10°. The substrates were placed horizontally in a substrate holder having a rotation feature to ensure uniform film deposition. The vertical and horizontal positions of the center of the substrate holder with respect to the target were 9.8 and 1.7 cm, respectively. The substrates were cleaned consecutively in acetone, isopropanol and deionized water and then baked at 200 °C to ensure complete dryness prior to deposition. All the layers were deposited using a fixed power of 40 W and a constant pressure of 0.3 Pa. Low power was used to avoid film surface damage due to the highly energetic ions typically associated with high power deposition [12]. To study the effect of the W dopant, different In_2O_3 ceramic targets of 5 cm in diameter (from Able Target Limited) containing 0, 0.5, 1.0, 1.6, 2.2, and 3.6 at% of W in the form of WO_3 were used. Rutherford backscattering spectrometry (RBS) of the films deposited on c-Si substrates was performed with 2-MeV He^+ ions from a van de Graaff accelerator to estimate the elemental content of the samples. Series of samples using different oxygen dilution percentage in the Ar sputtering gas ($[O_2]/[Ar + O_2] \times 100$ %, referred to as O_2-dilution hereon), from 0 to 2.2 %, were prepared for each differently doped sputtering target. The films of the thickness series were deposited at a constant W-doping level of 0.5 at% and O_2 dilution fraction of 1 %. All the layers, except those belonging to the thickness series, were deposited with constant deposition time of 107 min. The thicknesses of the deposited films were measured using RBS and a Bruker Dektak XT profilometer. The crystalline structures of the thin films were analyzed with X-ray diffraction (XRD) using Cu K_α radiation in the Bragg–Brentano geometry (Bruker D8 Discover). The optical transmission and reflection of the deposited films were measured using a Perkin Elmer Lambda 1050 double-beam spectrometer in the wavelength region from 200 to 2000 nm. The electrical resistivity (ρ) of the samples was measured using a Veeco FPP-100 four-point probe setup. A Hall effect measurement setup was used to determine carrier concentration (n) and carrier mobility (μ) of the films in the van der Pauw configuration using a 1.2 T electromagnet [17]. Scanning electron microscopy (SEM) was done with a FEI Magellan 400 instrument to visualize the surface and cross-sectional structure of the films.

3 Results

RBS spectra of In_2O_3 films deposited at room temperature from targets of different W concentrations at a constant oxygen dilution fraction of 0.5 % in Ar are shown in Fig. 1. The channel number scale of the x-axis can be converted to an energy scale of the backscattered α particles and to a mass scale of the scattering element [18]. In the spectra, the first feature appearing from large to small channel numbers is the W line, appearing as a shoulder on the right flank of the In line (channel ~390 to ~460) due to the limited mass resolution of RBS. The continuous spectrum from the Si substrate starts at channel number ~280, and the oxygen line appears on top of this continuum between channel ~160 and ~180. The atomic concentrations of the W dopant in the films extracted from these measurements using the RUMP software [19] are 0.5, 1.0, 1.8, 2.2 and 3.6 at%. These concentrations in at% can be converted to concentrations in atoms/cm^3 using the conversion factor of 7.8×10^{20} (at/cm^3)/(at%). The In and O concentrations are constant within the uncertainties (5 % for In and 20 % for O) for the different W concentrations, and result in the correct stoichiometry for In_2O_3. The oxygen concentration of the films did not change within the uncertainty of the measurements upon varying the oxygen dilution fraction. From the RBS spectra, it appears that the thicknesses of the films are 160 ± 10 nm. This thickness is in agreement with that determined using profilometry. The typical deposition rate for the samples in this study was 1.5 ± 0.12 nm/min.

Figure 2 demonstrates the electrical properties of the 0.5 at% W-doped films with variable thicknesses, deposited with 1 % O_2 dilution fraction in the sputtering gas. The

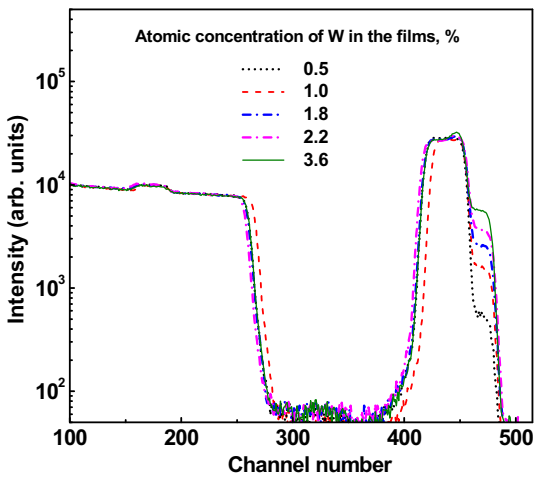

Fig. 1 RBS spectra of the W-doped In_2O_3 layers deposited on c-Si substrates from In_2O_3 targets containing different amounts of WO_3; the O_2-dilution fraction is 0.5 %

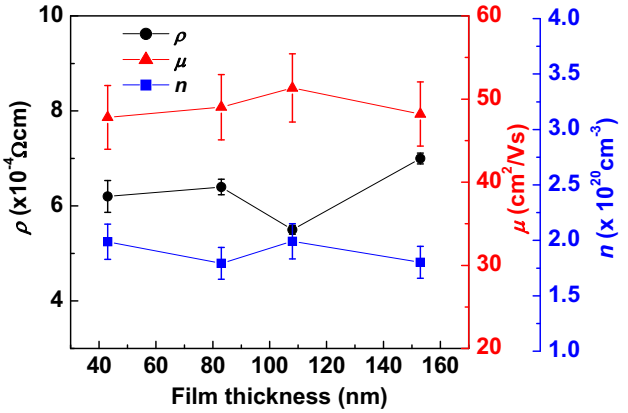

Fig. 2 The dependence of electrical properties of the IWO films on the thickness. The layers possess 0.5 at% W-doping level and are deposited with 1 % O_2-dilution fraction in the sputtering gas

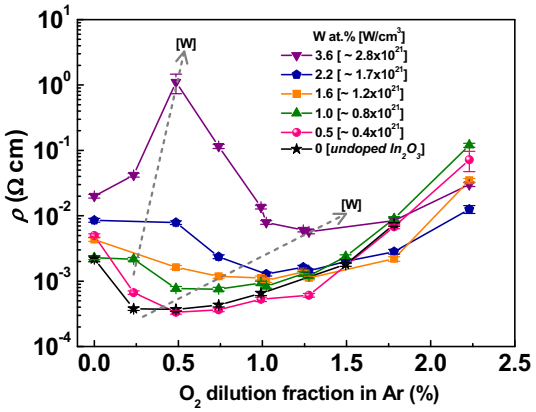

Fig. 3 The electrical resistivity of undoped and W-doped In_2O_3 films of different doping level versus the O_2-dilution fraction. The *dashed arrows* indicate the direction of increasing W doping

increase in the thickness from 43 to 108 nm leads to a small increase in mobility (from 48 to 51 cm^2/Vs), which results in a minor decrease in resistivity from 6.2×10^{-4} Ω cm to 5.5×10^{-4} Ω cm. The subsequent increase in the film thickness from 108 to 153 nm leads to a minor decrease in mobility (from 51 to 48 cm^2/Vs) and a corresponding increase in bulk resistivity (from 5.5×10^{-4} Ω cm to 7×10^{-4} Ω cm).

Figure 3 shows the dependence of the electrical resistivity of the In_2O_3 and IWO thin films as a function of both the W concentration and O_2-dilution fraction in Ar, measured by the four-point probe setup. It appears that in the higher W-doped films the resistivity initially rises with increasing oxygen dilution fraction, then falls until an oxygen dilution fraction of ~1.25 %, and rises slowly again for higher oxygen dilutions. As the W-doping level is decreased, the initial peak in the resistivity value is blunted and its position shifts toward lower O_2-dilution levels till it

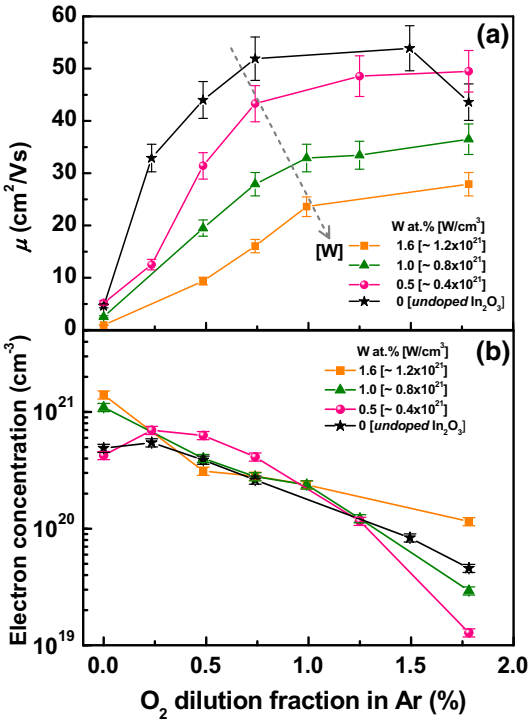

Fig. 4 **a** Electron mobility of undoped and W-doped In_2O_3 thin films of different doping levels for different O_2-dilution fraction (the *arrow* indicates the direction of increase of W in the films); **b** electron concentration of undoped and W-doped In_2O_3 films for different doping levels as a function O_2-dilution fraction

disappears for very low doping levels. For the undoped and low W-doped samples, on increasing the O_2-dilution fraction, the resistivity first decreases and then increases. The spread in resistivity is almost 4 orders of magnitude for an O_2-dilution fraction of ~0.5 % but reduces to about a factor of 2 for an O_2-dilution fraction of 1.5 %. The minimum resistivity is obtained for an O_2-dilution fraction of 0.5–1 % and a W concentration ≤0.5 at%, attaining a value of 3×10^{-4} Ω cm. The minima of the resistivity values are seen to shift to higher O_2-dilution levels for increasing W-doping levels, as shown by the dashed line. It is also seen that the rise of resistivity is sharper for the films with lower doping levels at higher oxygen dilutions, thus creating a crossover point of intersection, where at an oxygen dilution level of ~1.25 % all the films show a resistivity of $\sim 10^{-3}$ Ω cm.

Figure 4 shows results from the Hall effect measurements. The carrier mobility, displayed in Fig. 4a, increases strongly by almost a factor of 10 when the O_2-dilution fraction is increased from 0 to ~1 % for all the films, doped and undoped. It appears, however, to level off to constant values for high O_2-dilution fractions, within the range of our experimental study. Although the sharp rise in the mobility is seen with all the films, an increase in the doping level leads the rise in mobility to be more gradual

with a delayed onset of the plateau phase of the mobility. For constant O_2-dilution fraction, the carrier mobility drops with increasing W concentration. In the case of an O_2-dilution fraction of 0.75 %, the mobility decreases from a value of about 50 cm^2/Vs for an undoped layer to a value of about 10 cm^2/Vs for a W concentration of 2.2 at%. For the undoped film, there is a tendency of a drop in mobility at the highest O_2-dilution fraction. Figure 4b shows the dependence of the electron concentration of the In_2O_3 and IWO thin films on both the O_2-dilution fraction and the W concentration. The general trend for all W concentrations is that the electron concentration decreases with increasing O_2-dilution fraction, although a slight increase in the electron concentration with increasing O_2-dilution fraction is observed for the smallest doping levels at low O_2-dilution fraction. In some of the samples having high resistivity, Hall effect measurements were not possible because the low Hall voltage signals could not be discerned in the presence of the high resistive voltage signals. Having seen separately the factors influencing the electron mobility and electron concentration, it would be interesting to explore the dependence of electron mobility on the electron concentration, which is presented in Fig. 5. The electron mobility in both the doped and undoped In_2O_3 films shows a general rising trend with decreasing electron concentration, till around a value of $n \approx 3 \times 10^{20}$ cm^{-3}, where the rise in mobility slows down. For the electron concentrations below this threshold, there is a marked difference among the behavior of the different films. For the heavily W-doped film, there is still a gentle rise in the mobility with falling electron concentration. For the less doped films, this region shows more or less a plateau behavior for the mobility values. However, for the undoped In_2O_3 film, the mobility falls sharply at low electron concentrations, $n \approx 3 \times 10^{19}$ cm^{-3}. The reduction in the electron concentrations for these films was effectuated by increasing the O_2-dilution in Ar. In the same figure, at high carrier concentration values, a shaded region in the graph is shown where we see a completely different behavior of mobility versus carrier concentration for the films deposited without O_2. Here, the different films in spite of their very different doping concentrations have a very slow rise in mobility with decreasing electron concentration.

Optical transmission spectra of the different films are shown in Fig. 6a, b. The transmission as a function of wavelength, for films deposited with different doping levels but with a constant O_2-dilution fraction of 0.75 % in Ar, is shown in Fig. 6a. We can see a tendency of the average transparency of the films in the visible (400–800 nm) and the NIR (800–2000 nm) regions of light to decrease with increasing doping levels. The average visible transparency of 83 % and the average NIR transparency of 82 % for an undoped film decrease to 74 and 68 %, respectively, for a film doped to 2.2 at% W. Figure 6b shows the optical transmission of the films deposited with different O_2-dilution fraction but a constant W-doping level of 0.5 at%. Here the visible and NIR transparencies increase strongly with increasing O_2-dilution fraction. Visible and NIR light

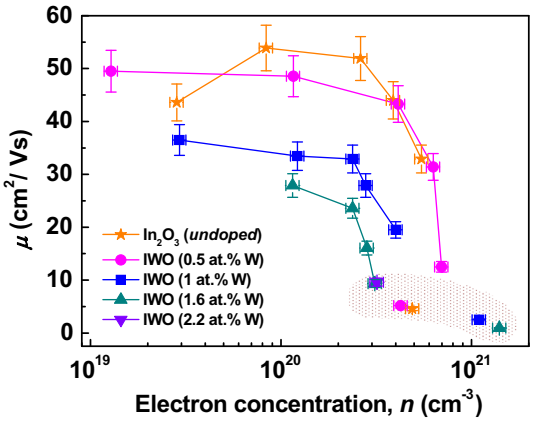

Fig. 5 Dependence of mobility on electron concentration for In_2O_3:-W films with different electron concentration. Separate data points on the *right down corner* represent the layers deposited with no oxygen intentionally introduced into the sputtering chamber

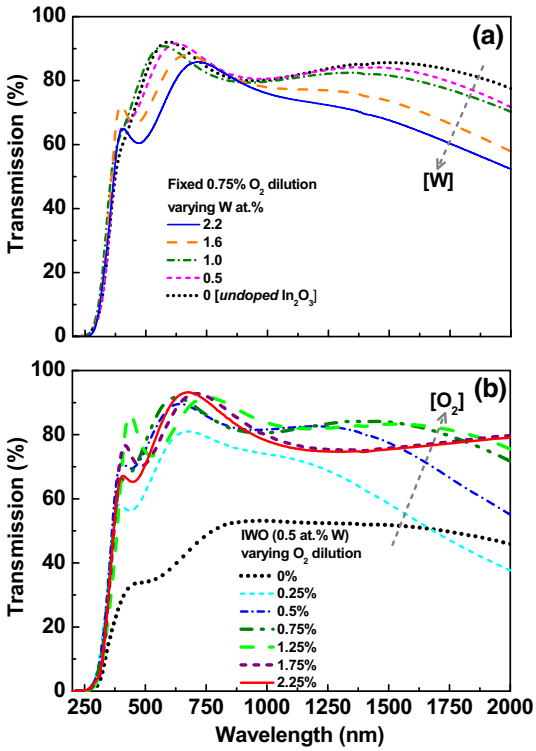

Fig. 6 **a** Optical transmission spectra of undoped and W-doped In_2O_3 films of different doping concentrations deposited at a constant O_2-dilution fraction of 0.75 %; **b** optical spectra of W doped (0.5 at%) In_2O_3 films deposited for different O_2-dilution fraction in Ar

transparency values of ~50 % for 0 % O_2-dilution fraction increases markedly even with a small amount of O_2-dilution reaching an average of 80 % for O_2-dilution fraction range of 0.75–1.25 %.

The optical absorption coefficient (α) of the films was determined from transmittance (T) and reflectance (R) by using reflectance corrected transmission, $T/(1-R) \approx e^{-\alpha d}$, which eliminates the optical interference effect arising from the film thickness (d) [20]. The optical energy gap, E_g, was determined from the analysis of the absorption coefficient near the optical absorption edge using the expression: $(\alpha h\nu) = A\,(h\nu - E_g)^{1/2}$, where A is a constant, h is the Planck constant, and ν is the frequency of the light, and a directly allowed electronic transitions for the IWO films are assumed [20]. The value of the energy gap can be extracted from the plot of $(\alpha h\nu)^2$ versus $h\nu$ as the x-intercept of the linear region of the curve. This is demonstrated in Fig. 6a for two different samples, one undoped In_2O_3 film and one doped IWO (2.2 at% W) film, both deposited at the same 0.75 % O_2-dilution level. The direct bandgap of undoped In_2O_3 was found to be 3.77 eV, which is close to the value of 3.75 eV observed in bulk indium oxide [21]. The extracted bandgap of the sample with 2.2 at% W doping is 3.99 eV. The dependence of the bandgap of IWO films (0.5 at% W) prepared with varied O_2-dilution is plotted in Fig. 7b. The bandgap value of the film deposited without any O_2 rises abruptly with a small addition of O_2 (0.25 %), but further addition of O_2 in the films reduces the bandgap values. Figure 7c shows a monotonic behavior of the rise in the bandgap values with an increase in the W-doping concentration (for a fixed 0.75 % O_2-dilution) in the film.

Figure 8a, b displays, respectively, the XRD patterns of undoped In_2O_3 and doped (1.6 at% W) IWO films, and each deposited at two different O_2-dilution fractions of 0 and 0.5 %. The peaks at 30° correspond to diffraction from the indium oxide bixbyite (222) plane, and the humps centered at 31.5° correspond to diffraction from amorphous indium oxide. The effect of the oxygen on the film microstructure is clearly evident with the disappearance of the diffraction peak in both the doped and undoped films deposited in 0.5 % of oxygen dilution. The diffraction peak of (222) in the case of doped IWO films has lower intensity and large FWHM compared to the (222) peak in the case of undoped In_2O_3 film, indicating that doping affects the crystallinity of the film and reduces the size of the crystallites. The cross-sectional images of these films taken by SEM are shown in Fig. 9, where (a) and (b) correspond to undoped films deposited in 0 and 0.5 % O_2-dilution, respectively, and (c) and (d) correspond to the IWO films deposited in 0 and 0.5 % O_2-dilution, respectively. The trends observed in the XRD analysis are corroborated by the SEM pictures, and a smooth surface with the absence of grains is seen in both the films with 0.5 % O_2-dilution (Fig. 9b, d). In contrast,

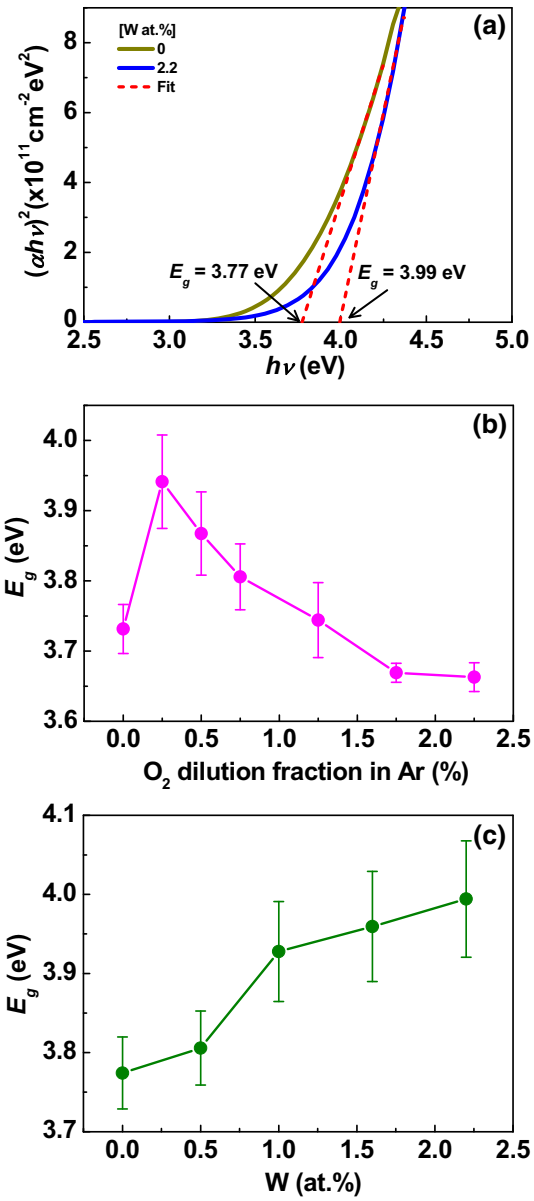

Fig. 7 **a** $(\alpha h\nu)^2$ versus $h\nu$ curves for In_2O_3 films with two different doping levels (undoped and 2.2 at% W) deposited with fixed 0.75 % O_2-dilution fraction; **b** dependence of the optical bandgap of In_2O_3:W (0.5 at% W) films with varying O_2-dilution; **c** dependence of optical bandgap on W-doping level for the In_2O_3:W films deposited at fixed 0.75 % O_2-dilution fraction

nanosized grains are visible in Fig. 9a, c for the undoped and doped samples with 0 % O_2-dilution fraction, with the grain sizes being visibly smaller in the case of doped film.

4 Discussion

The electrical and optical properties of metal oxide thin films are sensitive to the film thickness due to the accompanying microstructural changes and variations in defect

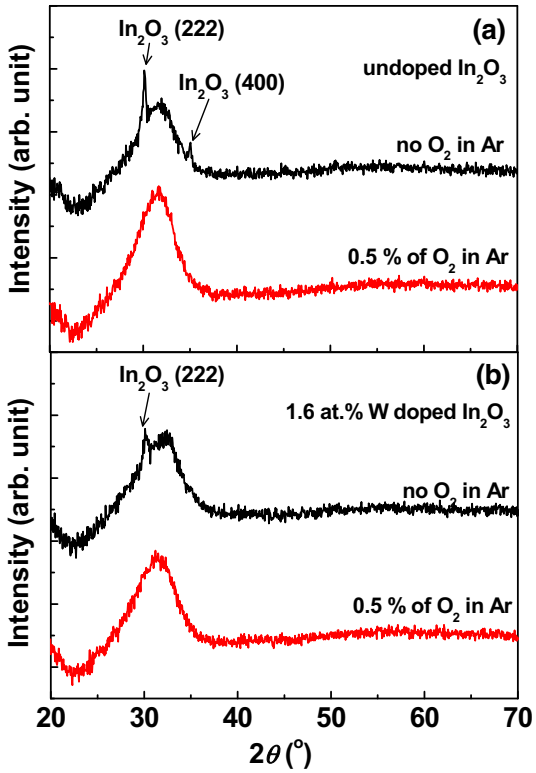

Fig. 8 X-ray diffraction patterns of undoped In_2O_3 films (**a**), and In_2O_3:W (1.6 at% W) films (**b**), deposited at different O_2-dilution fraction

densities with film growth [22, 23]. After an initial incubation layer, often disordered, at the interface between the substrate and the film, uniform microstructure and optoelectronic properties can be achieved till a certain thickness of the film. Large thicknesses again may give rise to problems of internal stress, microscopic defects, and deterioration of optoelectronic properties [22]. In our study, only minor changes in the electrical properties, namely $\sim$5 % change in mobility and carrier density, were observed in the series of films deposited with thicknesses varying from 43 to 153 nm (0.5 at% W-doped target with oxygen dilution fraction of 1 %), as seen in Fig. 2.

The influence of oxygen dilution levels and doping on the resistivity and electron mobility is demonstrated in Figs. 3 and 4a, respectively. Similar trends of the variation in resistivity with O_2-dilution have been reported in previous studies for isolated cases of room-temperature-deposited IWO films: the shallow U-shaped curve in a low-doped material [15] and inverted V-shaped peak in high-doped material [16]. Interestingly, the shifting of the minimum values of the resistivity in Fig. 3 and peak values of the mobility in Fig. 4a toward higher O_2-dilution with the rising W-doping levels bring out the importance of the balance between dopant concentration and oxygen vacancies in achieving IWO films with low resistivity.

Information on the carrier concentration can further clarify the interinfluence between the intrinsic oxygen vacancies and the external W dopants, both being sources of free electrons in doped In_2O_3 [24]. As shown in Fig. 4b, the electron concentration of the undoped film is 5.5×10^{20} cm^{-3} at the lowest O_2-dilution fraction and drops about a factor of 10 for the highest O_2-dilution fraction; this drop of electron concentration with an increasing O_2-dilution fraction is expected because the increased oxygen concentration reduces the number of oxygen vacancies. It is interesting to compare this behavior to that of the lowest doped IWO film (0.5 at% W): For 0 % O_2-dilution fraction, the carrier concentrations of the two films are equal; at slightly higher O_2-dilution fractions, the carrier concentration in the IWO film is almost twice that of the undoped film corresponding to a difference of $\sim 3 \times 10^{20}$ cm^{-3}; thus, a significant part of the 4×10^{20} W atom/cm^3 which have been added is electrically active. It cannot be concluded how big this fraction is as the distribution between W dopants donating 1 or 3 electrons is not known. At an O_2-dilution fraction of 1 %, the carrier concentrations in the two films become equal as the added oxygen deactivates the substituted W^{6+} ions by forming W–O complexes [5, 16, 25, 26]. The drop at the highest O_2-dilution fraction is largest for the doped film, indicating that the oxygen from the WO_3 might play a role in the deactivation process. At 0 % O_2-dilution fraction and for the highest W-doping concentration, the carrier concentration of the IWO films is significantly higher than that of the undoped film, about 1×10^{21} cm^{-3} corresponding approximately to the doping concentration. In accordance with the drop in electron concentration, the mobility increases by about a factor of 10 in the same range of O_2-dilution fraction, indicating that the ionized dopants play a significant role in the mobility. Thus, the crossover behavior in resistivity at higher oxygen dilution levels seen in Fig. 3 arises from the crossover behavior of the electron concentration, and not from the mobility behavior.

The effective electron mobility in general is influenced by various factors such as ionized impurity scattering, grain boundary scattering, and neutral impurity scattering [3, 27]. These factors in turn depend on the carrier concentration in the film and the film microstructure. In Fig. 5, the dependence of mobility of the undoped and doped In_2O_3 films with carrier concentration is shown. Here, the carrier concentration is highest, $\sim 10^{21}$ cm^{-3}, for samples deposited without any oxygen dilution and decreases with oxygen addition, showing a lowest of $\sim 10^{19}$ cm^{-3} at 1.75 % O_2-dilution. In Fig. 5, a complex behavior of μ versus n is observed, where the mobility of the films of each dopant series acquires a different path in spite of the underlying similarity in the general trend. Thus, it would be interesting to explore the scattering

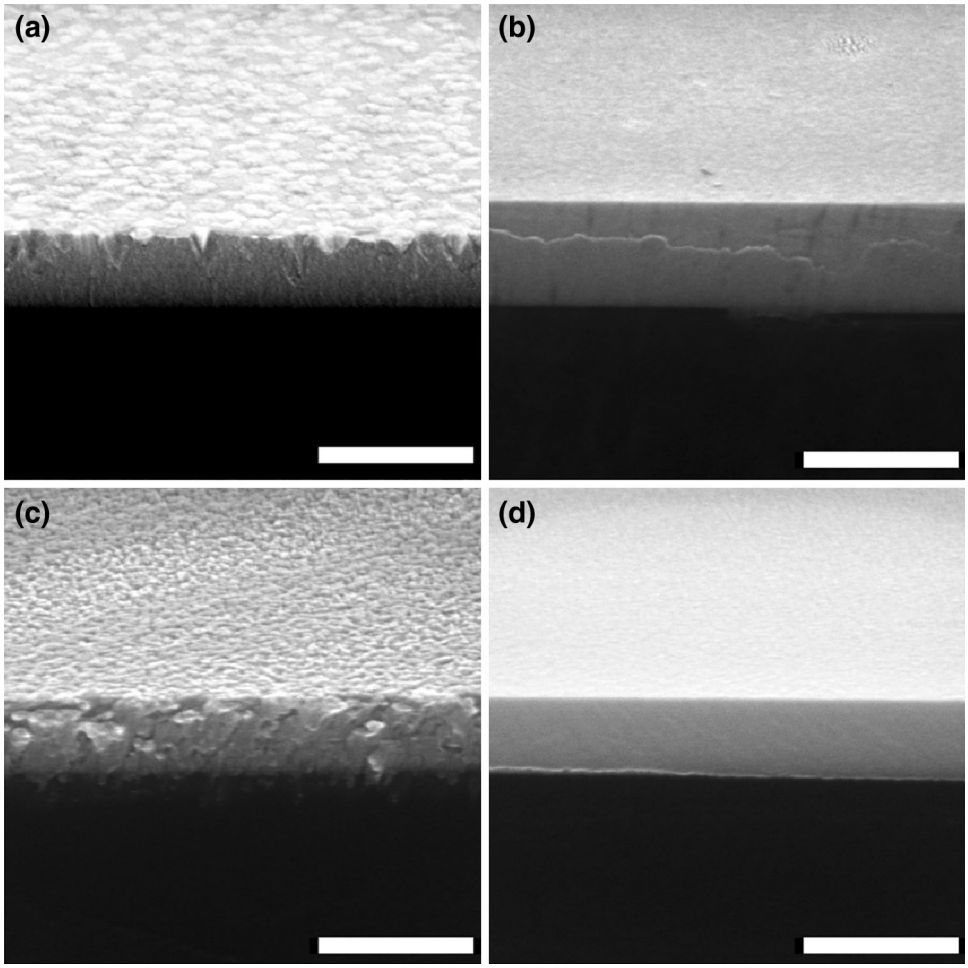

Fig. 9 SEM images (20° tilted) of the cross section of undoped and tungsten-doped indium oxide layers deposited on c-Si substrates with different O_2-dilution fraction: **a** undoped In_2O_3 without O_2; **b** undoped In_2O_3 with 0.5 % O_2-dilution; **c** In_2O_3:W (1.6 at% W) without O_2; **d** In_2O_3:W (1.6 at% W) with 0.5 % O_2. The length of white *scale bars* equals to 300 nm

mechanisms that are possibly responsible for the observed μ versus n behavior.

First, we consider the shaded region in the graph, which belongs to the films deposited without any O_2. The mobility in this distinct region shows a less steep rise with decrease in carrier concentration. This can be due to the reduced ionized impurity scattering. But even with almost one order of fall in carrier concentration, the mobility does not rise markedly. Therefore, we are led to deduce that some other factor must be at play in this region. The microstructure of the films in our study was found to be strongly dependent on the O_2-dilution fraction. Films deposited with O_2-dilution fractions from 0.5 to 1 % are found to be amorphous with smooth surfaces, while films deposited without oxygen show a nanocrystalline nature of the films and surface roughness (Figs. 8, 9). The effect of oxygen on the metal oxide film microstructure is brought about by the changes taking place in plasma chemistry and plasma energetics, and the variation in the flux and energies of the O^- ions. Electrons in the Ar/O_2 plasma attach to the electronegative oxygen atoms resulting in a decreased electron density, causing decreased collision numbers and increased electron temperature. In addition, the negative ions are accelerated in the cathode dark space, again leading to a small collision cross section. As a result, in the Ar/O_2 plasma, these high-energetic oxygen ions have a higher chance of impingement on the substrate and the growing film surface, leading to structural changes in the film [28–30].

The doping level was also found to be crucial for the microstructure of the films. Layers containing W (1.6 at%) have smaller grains than layers of undoped indium oxide as demonstrated by XRD and SEM in Figs. 8 and 9. In the case of crystalline films, like those prepared in O_2 deficient environment (the data in the shaded region of Fig. 5), the mobility also depends on the size of the crystallite grains and grain boundary potential. However, the rise in the mobility does not benefit from any contribution from the nanocrystallites because of their small sizes. Although the grain boundary scattering effect is insignificant in presence of high electron concentration, still it can play an important role in retarding the rise of mobility when the electron concentration is low enough [23].

Next, we consider the case of the doped and the undoped In_2O_3 films deposited in the presence of O_2, where we see an abrupt rise in the mobility with decrease in n. The decrease in n is mainly due to the incorporation of oxygen, which reduces the oxygen vacancies. It has been suggested that formation of complexes of W^{6+} substituting for In^{3+} and combining with interstitial O^{2-} leads to generation of a single carrier [16]. In such a scenario, initially the mobility rises on increasing the oxygen dilution due to formation of less electrically neutral complexes compared to the more carriers generated from activated W^{6+} ions or oxygen vacancies. The smaller number of electrically neutral complexes and low amount of impurities lead to decreased neutral complex scattering, an effect which increases the mobility of the existing carriers. Similar behavior was also reported for other transition metal-doped In_2O_3 materials [5, 25, 26]. Therefore, the rise in electron mobility in the low O_2-dilution range is due to the reduced ion scattering and less dominating neutral scattering centers in the lattice. However, beyond a certain threshold level of carrier concentration, $n \approx 2 \times 10^{20}$ cm^{-3}, which corresponds to a particular level of O_2, the mobility seems to saturate and stops rising. We recall that the films deposited in the presence of O_2 are amorphous in nature, and therefore, the applicability of grain boundary scattering is unlikely. However, it is known that the formation of neutral W^{6+} and W^{+4} complexes in the presence of excess oxygen can be the source of neutral impurity scattering. Similar arguments are also given for other transparent oxide systems [31].

Although these films are amorphous in nature, after a certain value of O_2 concentration, surface grains start forming. Impurities are prone to segregate at the grain boundaries. At very high O_2 concentration, conglomerates of amorphous grains are formed, leading to increased roughness of the film [31]. For example, in Fig. 10, where the SEM images of the surfaces of undoped films are shown, we see an abundance of large protruding amorphous grains in the film with 1.75 % O_2 ($\mu = 43$ cm^2/Vs) compared to the film with 1.5 % O_2-dilution ($\mu = 54$ cm^2/Vs). The XRD analysis of these grains showed them to be amorphous in nature (results not shown). The markedly different mobility values of these films are attributable to their distinct surface morphologies. The formation of such large amorphous grains does not occur for the range of O_2-dilution used in our study for doped IWO films because the extrinsic dopant W also acts toward the maintenance of an amorphous structure of the films. Oxygen segregation at the grain boundaries in the case of excess oxygen is commonly reported for the metal oxide system, where they can act as trap centers and capture the electrons and result in negatively charged scattering [3, 27, 31]. In the case of an undoped In_2O_3 system, negatively charged scattering at the grain boundaries can be one of the reasons for lowering the mobility, whereas in the W-doped In_2O_3 system, the possibility of both neutral and negatively charged scattering can be responsible for lowering the mobility. This explains the observed lower values of mobility for the W-doped In_2O_3 system compared to undoped system in our study, e.g., for a carrier concentration of 3×10^{20} cm^{-3}, the mobility of the films varies from 25 cm^2/Vs in IWO (1.6 at% W) to 54 cm^2/Vs in the undoped film.

Apart from the electrical properties, the other major aspect of TCOs is their optical properties. The O_2-dilution fraction drastically affects both the visible and the infrared (IR) transmission of the films (see Fig. 6b). At a fixed doping level, the transparency at the NIR region gradually increases with increasing O_2-dilution fraction, while the transmittance in the visible range increases up to a certain value of the O_2-dilution fraction (Fig. 6b) and then comes into saturation. Although the transmittance increases in both the visible and IR ranges with increasing oxygen dilution, the underlying mechanisms are different. When the deposition is carried out in an oxygen-less environment, indium suboxides of low oxidation number are expected to

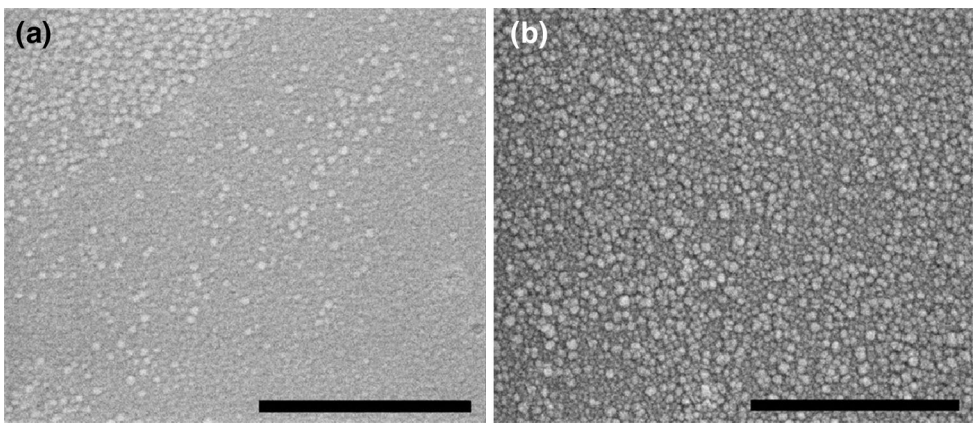

Fig. 10 SEM images of the surface of undoped indium oxide films deposited on glass with different oxygen dilution fractions: **a** 1.5 % and **b** 1.75 %. The length of *black scale bars* equals to 500 nm

be formed in the film, as observed in Ref. [14]. These species absorb light in the visible range, reducing the transmission of the films from ~85 % to 20–30 %. In contrast, when the deposition is carried out in an oxygen-rich environment, all the metal–metal bonds are expected to be saturated by oxygen, and the absorption in the visible range disappears. After the metal cations become fully surrounded with oxygen anions (the point where the transmittance in the visible range saturates), the carrier density starts to decrease due to the reduction in the number of oxygen vacancies. This decrease in carrier density (Fig. 4b) causes a shift of the plasma frequency toward lower values, causing an enhancement of the NIR transparency (Fig. 6b).

The optical and electrical properties are interlinked, and it is possible to understand one in the context of the other. The decrease in the NIR transmission with increasing doping level for constant O_2-dilution fraction of 0.75 % (Fig. 6a) is correlated with a drop of about a factor of 10 in the mobility (Fig. 3a) but with no strong change in the electron concentration (Fig. 4b). This increase in light absorption may be attributed to bound carrier absorption followed by excitation of electrons from the valence band to levels in the band gap originating from defects containing W. If these defects are charged, they will have a strong influence on the mobility. The initial decrease in the resistivity upon introduction of oxygen into the chamber (Fig. 3) is attributed to the observed increase in electron mobility (Fig. 4a) due to a saturation of the metal–metal bonds with oxygen, acting as scattering centers. The formation of metal–metal bonds at low oxygen/Ar ratios is also correlated with the optical properties of the layers as discussed above (Fig. 6b).

The variation in the band gap of IWO films with the level of O_2-dilution during the deposition of the film shown in Fig. 7b resembles the dependence of the carrier concentration of these films on O_2-dilution (Fig. 4b). This is due to the Burstein–Moss effect: A decrease in the free carrier density (Fig. 4b) causes a reduction in the energy of the higher occupied state in the conduction band of In_2O_3, thus decreasing the lowest energy of an optical transition [32, 33]. In the case of films deposited with varying W dopant but at fixed 0.75 % O_2-dilution, we see a monotonous rise in the band gap of the films with increasing W-doping concentration (Fig. 7c). This variation in band gap, however, does not follow any trend in respect of the respective carrier concentrations. Hence, the broadening in the band gap is not due to the Burstein–Moss effect as applicable in the previous case. Instead, this can be attributed to a decrease in the average In-O bonding length due to substitution of In with W in the amorphous network (the ionic radii for In^{3+} and W^{6+} ions in sixfold coordination state are 0.94 and 0.6 Å, respectively).

Apart from low resistivity and high optical transparency, specific microstructural attributes of TCOs can be beneficial for specific applications where post-deposition patterning is required. For instance, thin-film transistors, display panels, and organic light-emitting diodes require a smooth surface of the TCO, preferably an amorphous material. In recent times, a strong interest is shown for room-temperature-deposited In_2O_3–ZnO (IZO) films for such applications mainly because of its amorphous microstructure, even if the films have not yet shown a significantly low resistivity or high carrier mobility, especially at low thicknesses [1, 27]. In our study, the IWO films deposited with O_2-dilution fractions from 0.5 to 1 % are found to be amorphous with very smooth surfaces and possess best optical (visible and NIR transparencies of 83 and 80 %) and electrical properties (mobility of 45 cm^2/Vs). In this regard, our study has demonstrated the possibility of achieving low resistivity and high mobility along with amorphous microstructure in room-temperature-deposited IWO material even at low thicknesses using suitable combination of deposition conditions.

The IWO thin films we have developed have high carrier mobility and are depositable at low temperatures and can be used in solar cells on flexible plastic substrates, polymer solar cells, and low-temperature deposition of solar cell contacts. Apart from the high mobility, the high optical transparency in our IWO films is valuable for applications in multi-junction solar cells where a high transparency in the infrared part of the spectrum is desirable [9].

5 Summary

In the present investigation, the W-doping concentration and the O_2-dilution fraction in the Ar sputtering gas were varied during room-temperature rf-magnetron sputtering of a large number of In_2O_3 films. We studied the various series of these In_2O_3 films in order to distinguish and understand the contributions of free electrons from the oxygen vacancies and the W dopants, and the interrelationships between the optoelectronic properties and the underlying transport mechanisms. Electrically active W is only found for the combination of the highest doping concentrations and the lowest O_2-dilution fraction or for the lowest doping concentration and an O_2-dilution fraction between ~0.25 and ~1 %. For both the combinations, the maximal electrical activity is 100 % if it is assumed that each W atom donates one electron. We were able to develop IWO films at room temperatures having resistivity of 3.5×10^{-4} Ω cm, mobility of 45 cm^2/Vs, visible and NIR transparencies of 83 and 80 %, respectively, and with smooth surfaces. In our study, W-doping concentration below 1 at% and an O_2-dilution fraction above 0.75 %

yielded the best combination of optical and electrical properties. Different electrical, optical, and surface morphological properties result from different doping and oxygen dilution levels. Therefore, optimization of these two parameters can allow one to obtain IWO material with the desired characteristics depending on the intended application. Our study demonstrates that useful windows of optimum deposition conditions exist where the required material can be obtained in terms of low resistivity and high optical transparency, as well as microstructural features such as amorphous nature with smooth surface.

Acknowledgments This work has been supported by the Danish Strategic Research Council under the project named "Thin-film solar cells based on nanocrystalline silicon and structured backside reflectors—THINC." Thanks are due to John Lundsgaard Hansen for helping with XRD measurements, Sabrina R. Johannsen for help with the SEM measurements, Peter I. Gaiduk for help with the RBS measurements, and Kasper A. Borup for help with the Hall effect and resistivity measurements. Special thanks to Jacques Chevallier for helping with the rf-magnetron sputtering system.

References

1. D. Ginley, H. Hosono, D.C. Paine, *Handbook of transparent conductors* (Springer, Berlin, 2011)
2. F.-J. Haug, R. Biron, G. Kratzer, F. Leresche, J. Besuchet, C. Ballif, M. Dissel, S. Kretschmer, W. Soppe, P. Lippens, K. Leitner, Prog. Photovolt. Res. Appl. **20**, 727 (2012)
3. S. Calnan, A.N. Tiwari, Thin Solid Films **518**, 1839 (2010)
4. X. Li, Q. Zhang, W. Miao, L. Huang, Z. Zhang, Z.J. Hua, Vac. Sci. Technol. A **24**, 1866 (2006)
5. Y. Yoshida, T.A. Gessert, C.L. Perkins, T.J. Coutts, J. Vac. Sci. Technol. A **21**, 1092 (2003)
6. R.K. Gupta, K. Ghosh, P.K. Kahol, Appl. Surf. Sci. **255**, 8926 (2009)
7. Y. Meng, X.-L. Yang, H.-X. Chen, J. Shen, Y.-M. Jiang, Z.-J. Zhang, Z.-Y. Hua, Thin Solid Films **394**, 219 (2001)
8. E. Elamurugu, P. Shanmugam, G. Goncalves, N. Franco, E. Alves, R. Martins, E. Fortunato, Euro. Phys. Lett. **97**, 36002 (2012)
9. M. Balestrieri, D. Pysch, J.-P. Becker, M. Hermle, W. Warta, S.W. Glunz, Sol. Energy Mater. Solar Cells **95**, 2390 (2011)
10. J. De Wild, A. Meijerink, J.K. Rath, W.G.J.H.M. van Sark, R.E.I. Schropp, Energy Environ. Sci. **4**, 4835 (2011)
11. J.R. Bellingham, W.A. Phillips, C.J. Adkins, J. Phys. Condens. Matter **2**, 6207 (1990)
12. J. Pan, W. Wang, D. Wu, Q. Fu, D. Ma, J. Mater. Sci. Technol. **1**, 1 (2013)
13. Y. Sato, R. Tokumaru, E. Nishimura, P.-K. Song, Y. Shigesato, K. Utsumi, H. Iigusa, J. Vac. Sci. Technol. A **23**, 1167 (2005)
14. E. Elangovan, R. Martins, E. Fortunato, Thin Solid Films **515**, 8549 (2007)
15. Y. Abe, N. Ishiyama, H. Kuno, K. Adachi, J. Mater. Sci. **40**, 1611 (2005)
16. Z. Lu, F. Meng, Y. Cui, J. Shi, Z. Feng, Z. Liu, J. Phys. D Appl. Phys. **46**, 075103 (2013)
17. K.A. Borup, E.S. Toberer, L.D. Zoltan, G. Nakatsukasa, M. Errico, J.-P. Fleurial, B.B. Iversen, G.J. Snyder, Rev. Sci. Instrum. **83**, 123902 (2012)
18. L.C. Feldman, J.W. Mayer, *Fundamentals of Surface and Thin Film Analysis* (North-Holland, New York, 1986)
19. L.R. Doolittle, Nucl. Instrum. Methods Phys. Res. Sect. B **9**, 344 (1985)
20. Y. Hishikawa, N. Nakamura, S. Tsuda, S. Nakano, Y. Kishi, Y. Kuwano, J. Appl. Phys. **30**, 1008 (1991)
21. R.L. Weiher, R.P. Ley, J. Appl. Phys. **37**, 299 (1966)
22. C.C. Kuo, C.C. Liu, Y.F. Jeng, C.C. Lin, Y.Y. Liou, J.L. He, J. Nanomater. **2010**, 840316 (2010)
23. Q. Zhang, X. Li, G. Li, Thin Solid Films **517**, 613 (2008)
24. Y.H. Lin, Y.S. Liu, Y.C. Lin, Y.S. Wei, K.S. Liao, K.R. Lee, J.Y. Lai, H.M. Chen, Y.C. Jean, C.Y. Liu, J. Appl. Phys. **113**, 033706 (2013)
25. M.F.A.M. Van Hest, M.S. Dabney, J.D. Perkins, D.S. Ginley, M.P. Taylor, Appl. Phys. Lett. **87**, 032111 (2005)
26. C. Warmsingh, Y. Yoshida, D.W. Readey, C.W. Teplin, J.D. Perkins, L.M. Gedvilas, B.M. Keyes, D.S. Ginley, J. Appl. Phys. **95**, 3831 (2004)
27. A.J. Leenheer, J.D. Perkins, M.F.A.M. van Hest, J.J. Berry, R.P. O'Hayre, D.S. Ginley, Phys. Rev. B **77**, 115215 (2008)
28. K. Tominaga, T. Yuasa, M. Kume, O. Tada, Jpn. J. Appl. Phys. **24**, 944 (1985)
29. K. Tominaga, K. Kuroda, O. Tada, Jpn. J. Appl. Phys. **27**, 1176 (1988)
30. K. Ellmer, J. Phys. D Appl. Phys. **33**, R17 (2000)
31. H.-C. Lee, O.O. Park, Vacuum **77**, 69 (2004)
32. E. Burstein, Phys. Rev. **93**, 632 (1954)
33. T.S. Moss, Proc. Phys. Soc. Lond. **B67**, 775 (1954)